

7-15-2007

Performance Analysis of a Ge/Si Core/Shell Nanowire Field-Effect Transistor

Gengchiao Liang
Harvard University

Jie Xiang
Harvard University

Neerav Kharche
Purdue University - Main Campus

Gerhard Klimeck
Purdue University - Main Campus, gekco@purdue.edu

Charles M. Lieber
Harvard University

See next page for additional authors

Follow this and additional works at: <https://docs.lib.purdue.edu/nanopub>

Liang, Gengchiao; Xiang, Jie; Kharche, Neerav; Klimeck, Gerhard; Lieber, Charles M.; and Lundstrom, Mark, "Performance Analysis of a Ge/Si Core/Shell Nanowire Field-Effect Transistor" (2007). *Birck and NCN Publications*. Paper 438.
<https://docs.lib.purdue.edu/nanopub/438>

This document has been made available through Purdue e-Pubs, a service of the Purdue University Libraries. Please contact epubs@purdue.edu for additional information.

Authors

Gengchiao Liang, Jie Xiang, Neerav Kharche, Gerhard Klimeck, Charles M. Lieber, and Mark Lundstrom

Performance Analysis of a Ge/Si Core/Shell Nanowire Field-Effect Transistor

Gengchiao Liang,^{*,†,‡} Jie Xiang,[‡] Neerav Kharche,[†] Gerhard Klimeck,[†]
Charles M. Lieber,^{‡,§} and Mark Lundstrom[†]

School of Electrical and Computer Engineering and Network for Computational Nanotechnology, Purdue University, West Lafayette, Indiana 47907, Department of Chemistry and Chemical Biology, Harvard University, Cambridge, Massachusetts 02138, and Division of Engineering and Applied Sciences, Harvard University, Cambridge, Massachusetts 02138

Received November 6, 2006; Revised Manuscript Received January 30, 2007

ABSTRACT

We analyze the performance of a recently reported Ge/Si core/shell nanowire transistor using a semiclassical, ballistic transport model and an $sp^3d^5s^*$ tight-binding treatment of the electronic structure. Comparison of the measured performance of the device with the effects of series resistance removed to the simulated result assuming ballistic transport shows that the experimental device operates between 60 and 85% of the ballistic limit. For this ~ 15 nm diameter Ge nanowire, we also find that 14–18 modes are occupied at room temperature under ON-current conditions with $I_{ON}/I_{OFF} = 100$. To observe true one-dimensional transport in a $\langle 110 \rangle$ Ge nanowire transistor, the nanowire diameter would have to be less than about 5 nm. The methodology described here should prove useful for analyzing and comparing on a common basis nanowire transistors of various materials and structures.

Semiconducting nanowire transistors are attracting attention due to their potential applications such as electronics^{1–7} and biomolecule detection.^{8,9} Promising device performance has recently been reported for Si^{2,6} and Ge¹ nanowire field-effect transistors (NWFETs). High hole/electron mobilities, large ON-currents, large I_{ON}/I_{OFF} ratios, and good subthreshold swings have been reported.^{1,2,5,6} These device performance metrics provide important measures of progress as device fabrication technologies are being refined, but it is still unclear how measured results compare against theoretical expectations, how to compare the results from different experiments, and how to assess nanowire transistor performance against that of state-of-the-art silicon metal oxide semiconductor FETs (MOSFETs). Mobility is commonly used as a device metric, but it is not a well-defined concept at the nanoscale, and its relevance to nanoscale MOSFETs is unclear. It is more appropriate to compare a nanoscale MOSFET against its ballistic limit. In this letter, we do so by analyzing the performance of a recently reported Ge/Si core/shell NWFET.¹

We analyze the performance of a NWFET by comparing the measured current vs voltage (I – V) characteristics to a theoretical model of a ballistic nanowire MOSFET. This semiclassical, top-of-the-barrier model requires as inputs the electronic structure of the nanowire and the gate and drain capacitances.¹⁰ To obtain the bandstructure of the Ge nanowire, we assume an unrelaxed nanowire atomic geometry with bulk atomic positions and construct the Hamiltonian of the nanowire unit cell using the orthogonal-basis $sp^3d^5s^*$ tight-binding method developed for bulk electronic structure.¹¹ Each atom is modeled using 10 orbitals per atom per spin (20 orbitals per atom total). The parameters in this tight-binding model were fit by a genetic algorithm to reproduce the band gap and the electron/hole-effective masses in the different valleys.¹¹ The simulated nanowire is assumed to be infinitely long, and the nanowire surface is taken to be passivated by hydrogen atoms, which are treated numerically using a hydrogen termination model of the sp^3 hybridized interface atoms.¹² This technique has been reported to successfully remove all the interface states from the band gap.¹² Although no relaxation or strain effects are included, this model has shown good agreement with the measured band gap vs diameter of silicon nanowires.¹³ For large diameter nanowires such as the one under investigation here ($d \sim 15$ nm), the subband separation is only few meV, so

* Corresponding author. E-mail: elelg@nus.edu.sg.

[†] School of Electrical and Computer Engineering and Network for Computational Nanotechnology, Purdue University.

[‡] Department of Chemistry and Chemical Biology, Harvard University.

[§] Division of Engineering and Applied Sciences, Harvard University.

[‡] Current address: Department of Electronic and Computer Engineering, National University of Singapore, Singapore.

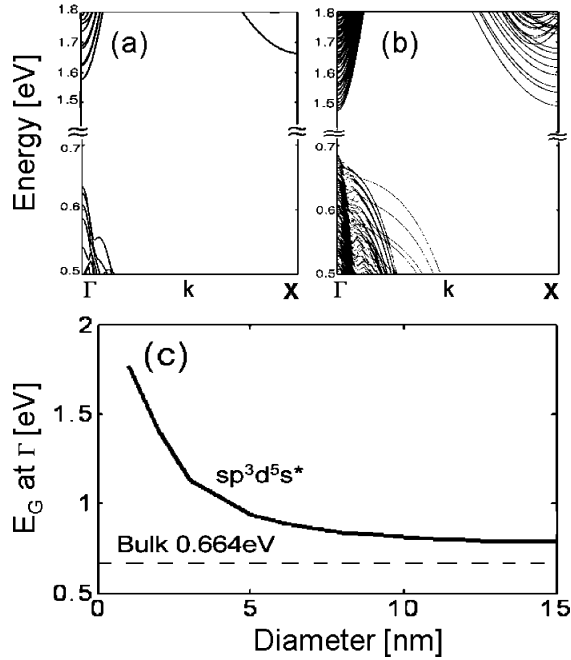


Figure 1. (a and b) Electronic structure of the $D = 5$ and 15 nm $\langle 110 \rangle$ cylindrical Ge nanowire, respectively. (c) Band gap E_G as function of diameter for a cylindrical $\langle 110 \rangle$ Ge-nanowire where E_G is taken at the Γ -point of the 1D Brillouin zone. When the diameter of the nanowire is less than 5 nm, the band gap shows a significant increase.

that the electronic properties of the nanowire should be well described by this tight-binding approach.

Parts a and b of Figure 1 display the computed band structure for 5 and 15 nm diameter (D) $\langle 110 \rangle$ Ge nanowires. Because of quantum confinement, the direct band gap at the Γ -point (projection of L valley of bulk Ge bandstructure) of the nanowire is larger than the indirect band gap of bulk Ge and increases as the diameter of nanowire decreases, as shown in Figure 1c. A similar phenomenon in Si nanowires has been theoretically predicted by different studies.^{14,15} The results shown in Figure 1c indicate that, in order to see significant quantum confinement effects, the diameter of the nanowire should be smaller than about 5 nm.

To simulate the ballistic I - V characteristics of NW MOSFETs, a semiclassical top-of-the-barrier MOSFET model was used.¹⁰ In this model, a simplified three-dimensional self-consistent electrostatic model including quantum capacitance effects is coupled with a ballistic treatment of hole transport. Three-dimensional electrostatics is described by a simple capacitance model.¹⁰ The capacitors represent the electrostatic coupling of the gate (C_G), drain (C_D), and source terminals (C_S) to the top of the potential barrier at the source end of the channel. These capacitors control the subthreshold swing, S , of the transistor and the drain-induced barrier lowering (DIBL) according to

$$\frac{C_G}{C_\Sigma} = \frac{2.3k_B T/q}{S} \quad (1a)$$

$$\frac{C_D}{C_\Sigma} = \frac{2.3k_B T/q}{S} \times \text{DIBL} \quad (1b)$$

$$C_\Sigma = C_G + C_D + C_S \quad (1c)$$

The gate insulator capacitance is the most critical parameter in this model. The maximum capacitance would be achieved in a cylindrical gate geometry, as shown in Figure 2a. For top-gated devices, however, a half-cylinder geometry as shown in Figure 2b may be a closer approximation to the actual structure. We used the finite element package, FEMLAB, to compute the theoretical capacitance for such a structure. In practice, the actual capacitance may be difficult to estimate because of uncertainties in film thicknesses and in the geometry of the gate stack. Measurement of the actual gate capacitance on the specific device being analyzed would be the best procedure, but such measurements are difficult. (Very recently similar measurements on a carbon nanotube transistor have been reported.¹⁶) Accordingly, we will consider both the cylindrical and half-cylindrical geometries in the analysis that follows. The uncertainty in gate capacitance is one of the most significant contributions to the error bars for our analysis.

The Poisson's potential (U_{SCF}) is equal to $U_0(N - N_0)$, where $U_0 = q/C_\Sigma$ is the single electron charging energy, N_0 and N are the number of mobile carriers at the top of the barrier at equilibrium and under applied bias, respectively, and C_Σ is the total capacitance. The carrier density, N , moreover, can be directly computed from the previously determined E - k relations,

$$N = \int_{-\infty}^{\infty} \frac{dk}{\pi} [f(E(k) + U_{scf} - E_{fs}) + f(E(k) + U_{scf} - E_{fs} + qV_D)] \quad (2)$$

where $f(E)$ is the Fermi function and E_{fs} is the chemical potential in the source region. Iteration between N and U_{scf} is repeated until the self-consistency reaches convergence. The NW MOSFET current is then evaluated using the semiclassical transport equation in the ballistic limit:

$$I = \frac{2q}{h} \int_{U_{scf}}^{\infty} dE [f(E - E_{fs}) - f(E - E_{fs} + qV_D)] \quad (3)$$

More details of this model can be found in refs 10 and 17.

Using the techniques described above, we analyzed the performance of a recently reported Ge/Si core/shell nanowire FET.¹ The nominal diameter of the Ge core is $D = 14.7 \pm 2$ nm, and the axial crystallographic direction of the nanowire is along $\langle 110 \rangle$. The gate insulator consists of a layer of HfO_2 deposited by atomic layer deposition, a SiO_2 native oxide layer, and the depleted silicon shell layer. Any doping of the silicon shell layer would simply shift the threshold voltage of the device, but threshold voltage differences are removed by the analysis procedure. The thickness of each insulator shell in this simulated device is taken to be 4 nm, 1 nm, and 1.7 nm for HfO_2 ($\kappa = 23$), SiO_2 ($\kappa = 3.9$), and Si ($\kappa = 11.9$) shell, respectively, as determined from the fabrication process. The nanowire sits on a 50 nm thick layer of SiO_2 on top of an n-type silicon wafer doped with

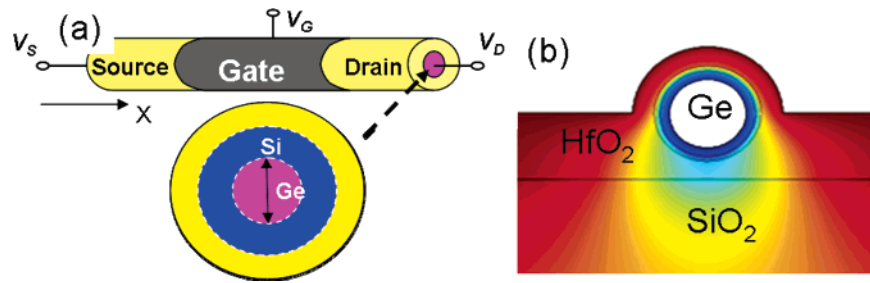


Figure 2. Schematics of a cylindrical gate nanowire (a) and a half-cylindrical gate nanowire sitting on the SiO₂ substrate (b).

resistivity less than 0.005 Ωcm. Using these numbers, we obtain a gate insulator capacitance as $6.9 < C_G < 10.7$ pF/cm. The device to be analyzed has a channel length of 190 nm. For details of the fabrication process and device structure, see ref 1.

Because of uncertainties in threshold voltage caused by charge at the dielectric/semiconductor interface and the work functions of different gate electrodes, it is not advisable to compare $I-V$ characteristics of devices directly. It is preferable to compare I_{ON} vs I_{ON}/I_{OFF} at a fixed drain voltage.¹⁸ To generate such a curve from measurements or theoretical calculations, the supply voltage, V_{DD} , is first specified. For this analysis, we take $V_{DD} = 1$ V. From the measured or calculated drain current as function of V_{GS} for $V_{DS} = V_{DD}$, we extract I_{ON} vs I_{ON}/I_{OFF} by defining a “window” V_{DD} volts wide and superimposing it on the $I-V$ characteristic. We then read I_{ON} from the left side of the window and I_{OFF} from the right side. By sweeping the window across the entire $I-V$ characteristic, we produce a plot of I_{ON} vs I_{ON}/I_{OFF} .

Figure 3a shows the experimentally measured (symbols) I_{DS} vs V_G at $V_D = 1, 0.1,$ and 0.01 V. The subthreshold swing at $V_D = 1$ V is 100 mV/decade. The DIBL is obtained as 150 mV/V from the horizontal displacement in the $V_D = 1$ and 0.1 V curves at $I_D = 0.1$ μA. The series resistance of this device can be obtained from the experimental I_D vs V_G characteristic at a low drain bias of $V_D = 100$ or 10 mV. The inset of Figure 3a shows the measured device resistance, $R_{SD} = \Delta V_{DS}/\Delta I_{DS}$, as a function of $-V_G$ for $V_D = 0.1$ V and 10 mV. The saturation value of $R_{SD} = 5.6$ kΩ appears between $V_G = 0$ to $V_G = -1$ V and is the series resistance of the device. This parameter is used in the calculations to adjust the voltage drop from the drain to the source as well as from the gate to the source, although the channel is still assumed ballistic.

Figure 3a also shows the comparison of the device transfer characteristics between the experimental data (symbols) of this Ge/Si core/shell FET and the simulated ballistic results (solid line) of a 13 nm diameter Ge nanowire MOSFET with a half-cylindrical gate. The Fermi level at equilibrium is set to 1.1 V below the top of the valence band of the nanowire. The experimental data is slightly larger than the theoretical, ballistic calculations below the threshold because the tunneling currents are not included in the semiclassical, ballistic transport model. At the device’s ON-state, however, the simulation results are larger than the experimental measurements, which we attribute to the inelastic scattering processes in the device. The scattering processes will degrade the

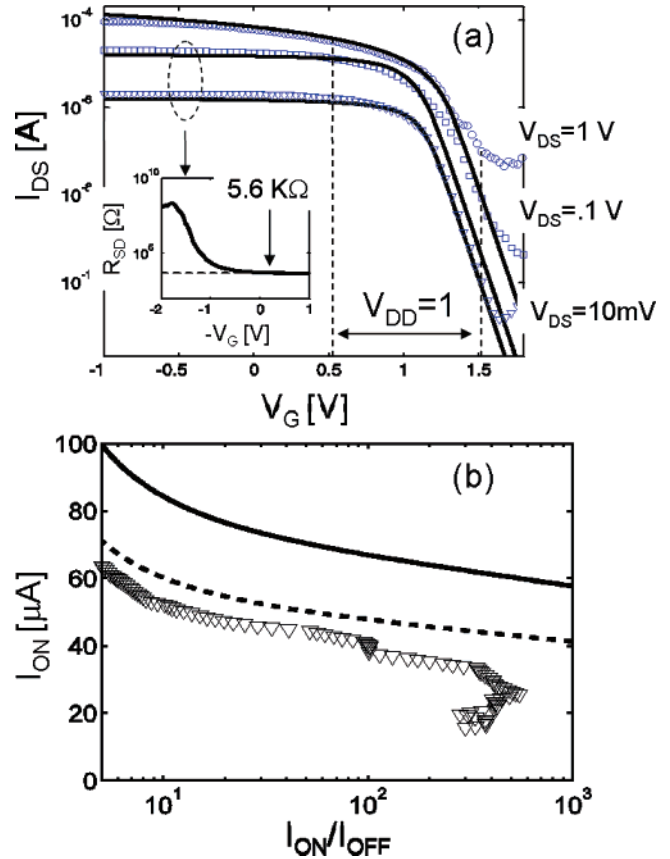


Figure 3. (a) Experimental measurements (symbols) of a $\langle 110 \rangle$ Si/Ge core/shell nanowire MOSFET: I_{DS} as a function of V_G at $V_D = 1, 0.1,$ and 0.01 V. The vertical dashed lines show the V_{DD} window used to obtain the dependence of I_{ON} on I_{ON}/I_{OFF} in Figure 3b. On the basis of the data of $V_D = 1$ V, $S = 100$ mV/decade can be determined. Using the data of $V_D = 0.1$ and 0.01 V, the dependence of R_{SD} on V_D can be calculated (inset). The flat region of R_{SD} can be attributed to the series resistance (at $V_G = 0$, $R_{SD} = 5.6$ kΩ). The solid line shows the simulated transfer characteristics of a 13 nm Ge nanowire MOSFET with a half-cylindrical gate. (b) Simulated ON-current vs I_{ON}/I_{OFF} for a $\langle 110 \rangle$ Ge NW MOSFET with $R_{SD} = 5.6$ kΩ in comparison with experimental data (triangles). Solid and dashed lines present the simulated ballistic results with $D = 17$ nm and $C_G = 10.7$ pF/cm, and $D = 13$ nm and $C_G = 6.9$ pF/cm, respectively.

device performance and reduce the currents in realistic devices.

The ambipolar behavior displayed in Figure 3a raises the possibility that this device is a Schottky barrier FET. The top-of-the-barrier models we use to analyze the data assume MOSFET-type operation in which the source can supply any current that the gate demands. Using an approach proposed

by J. Appenzeller et al.,^{19,20} we estimate that the barrier height of this device is only 30 meV, which may be small enough to ensure MOSFET-type operation.

Figure 3b compares the simulated I_{ON} vs I_{ON}/I_{OFF} for two ballistic Ge NW MOSFETs with a series resistance of 5.6 K Ω as compared to the experimental measurements (triangles). Because of uncertainties of the experimental device structure, two cases were considered. The solid line presents the maximum estimated ballistic $I-V$ of a Ge NW MOSFET with a perfectly cylindrical gate ($C_G = 10.7$ pF/cm) and the largest estimated diameter with $D = 17$ nm, whereas the dashed line presents the minimum possible ballistic $I-V$ of a Ge NW MOSFET with half-cylindrical metal gate ($C_G = 6.9$ pF/cm) and the smallest possible diameter with $D = 13$ nm. Our analysis shows that this nanowire transistor operates between 60 and 85% of the ballistic limit at $I_{ON}/I_{OFF} = 100$. Even with the most conservative assumption of a cylindrical gate, the device appears to operate rather close to the ballistic limit, while the more reasonable assumption of a half-cylindrical gate suggests that this device operates at its ballistic limit.

To gain further insight into the performance of this device, we first study the effects of the diameter of the nanowire and the shape of the gate on device performance. Figure 4a shows I_{ON} at a fixed $I_{ON}/I_{OFF} = 100$ vs the nanowire diameter for two different shapes of the gate. We found that ON-current of nanowire MOSFETs monotonically increases with the diameter of nanowire. This occurs because the subband separation monotonically increases as the diameter of the nanowire decreases, and the insulator capacitance also monotonically decreases as the nanowire diameter decreases. These two effects reduce the number of modes involved into carrier transport for the smaller diameter nanowires. When the diameter of the nanowire is smaller than 5 nm, however, the ON-current at a fixed I_{ON}/I_{OFF} starts increasing instead of decreasing. This unusual effect is due to the light-hole–heavy-hole splitting,¹³ which causes the hole-effective mass of the first few subbands to become lighter, which enhances the device performance. Similar phenomena have been predicted in ref 13. Finally, by simulating a device with different gate capacitance (by changing the gate shape as in Figure 4a or by changing the insulator thickness) for a given V_{DD} , the number of subbands populated and the ON-current with increase with C_G .

Second, the number of modes involved in carrier transport, i.e., the number of modes between E_{fs} and $E_{fs} - qV_D$ vs gate bias was studied for two different nanowire diameters. The outside shells, Si, SiO₂, and HfO₂, remain constant (same geometry as described above), and the Fermi level is set to 100 meV above the first valence subband at equilibrium for all cases in this simulation. Figure 4b shows the number of populated modes vs V_G for a small diameter (3 nm) and a large diameter (17 nm) Ge nanowire MOSFET with a perfectly cylindrical gate under $V_{DS} = 1$ V. We found that the number of populated modes strongly depends on the nanowire diameter and decreases as the diameter shrinks because of the larger subband separation in wires with smaller diameter. According to the geometry of the measured

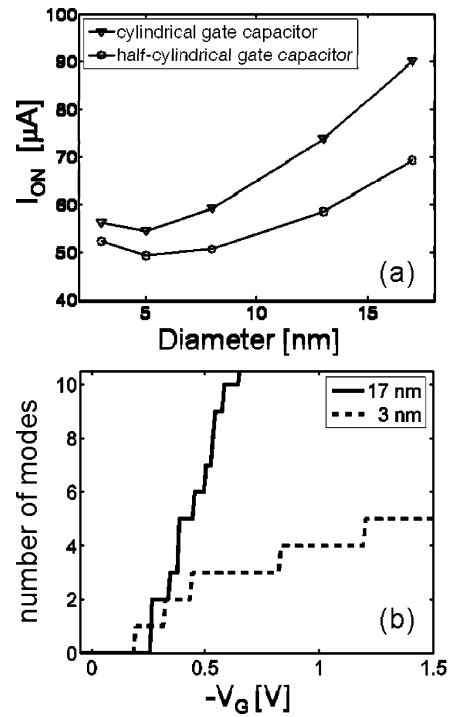


Figure 4. (a) I_{ON} at $I_{ON}/I_{OFF} = 100$ vs the nanowire diameter for the different gate shapes. The device performance monotonically increases with the diameter of the nanowire when the diameter of the nanowire is larger than 5 nm. When it is smaller than 5 nm, however, the device performance is enhanced due to the light-hole–heavy-hole splitting caused by the quantum confinement effects.¹³ (b) Dependence of the number of modes involved in carrier transport on the gate voltage for the 3 nm (dashed) and 17 nm (solid) diameter Ge nanowires under $V_{DS} = 1$ V. The outside shells, Si, SiO₂ and HfO₂, remain constant, and the Fermi level is set to 100 meV above the first valence subband for both cases in this simulation. Compared to a large diameter nanowire such as 17 nm diameter one, the small diameter nanowire (3 nm) is relatively feasible to observe true 1D transport at room temperature due to the larger subband separation.

device, the maximum and minimum possible number of subbands dropping between E_{fs} and $E_{fs} - qV_D$ under ON-current conditions for $I_{ON}/I_{OFF} = 100$ was determined to be 18 modes and 14 modes for the 17 nm diameter nanowire with a perfectly cylindrical gate and the 13 nm diameter with a half-cylindrical gate, respectively. The results show that, although conduction in this NWFET is not one-dimensional, a relatively small number of modes carry the current.

To observe true 1D transport at room temperature, the diameter of Ge nanowire MOSFET should be relatively small, such as 3 nm as shown in Figure 4b. For a large diameter (17 nm) nanowire MOSFETs, the number of populated modes increases quickly as soon as the device turns on. In the 3 nm case, however, the number of populated modes increases slowly as V_G increases, which provides a larger voltage margin to observe true 1D single-subband carrier conduction compared with larger diameter nanowires. Because scattering was not included in our ballistic simulations, we expect that more subbands would be populated for a given ON-current in actual devices. On the other hand, the number of populated modes would be overestimated by the ballistic simulation in the case of a given gate voltage. This occurs because, under modest drain bias in the ballistic

case, only the $+k$ states are occupied, and to balance the gate charge, a certain number of subbands will have to be populated. In the diffusive case, the $-k$ states are also occupied so that the required charge in the nanowire would be accommodated in a smaller number of subbands.

Our analysis of this experiment is based on a number of assumptions that should be carefully examined. First, there is the uncertainty in the precise gate capacitance, which can only be resolved by directly measuring the gate capacitance on the device under test. Second is our assumption of bulk atomic positions for the nanowire. Crystalline Si has a 4% lattice mismatch with Ge. Therefore, a large amount of strain might exist at the epitaxial core/shell interface. Although our preliminary examination of relaxation effects using NEMO-3D^{21,22} and a similar Ge/Si nanowire core/shell structure FET (but with $\langle 100 \rangle$ orientation) suggests that the ON-current does not vary substantially with introduction of interfacial stress, a more extensive study of strain relaxation on carrier transport resulting from the lattice mismatch in Ge/Si core/shell nanowire MOSFETs is underway. Finally, we have not treated the self-consistent band-bending within the nanowire itself, which could also affect the electronic structure. Each of these assumptions is being examined, but we do not expect the broad conclusions to change; this device appears to operate relatively close to the ballistic limit. In spite of the uncertainties, this result is surprising, given that a recent theoretical analysis suggests that silicon nanowire FETs should operate very far from the ballistic limit when the channel length is longer than only a few nanometers.²³ Additional experimental and theoretical investigations are needed to further address the nature of room-temperature high-field transport in nanowire transistors, specifically how they can operate so close to the ballistic limit.

In summary, recent experimental results for a Ge/Si core/shell NWFET device were analyzed, and the results suggest that this device operates surprisingly close to its ballistic limit. The device appears to operate as a nanowire MOSFET, with only about 14–18 modes involved in carrier transport. Our analysis also suggests that, to obtain true one-dimensional transport in a $\langle 110 \rangle$ Ge NW MOSFET, the nanowire diameter would have to be much less than about 5 nm, and the device bias would have to be carefully selected. More precise analyses of experimental data like this will require careful measurements of nanowire gate capacitance and an understanding of how lattice strain and self-consistent electrostatics affect the electronic structure of nanowires. In general, the methodology presented here should prove useful for analyzing and comparing on a common basis nanowire transistors of various materials and structures.

Acknowledgment. The work at Purdue was supported by the MARCO Focus Center on Materials, Structures, and Devices, the Army Research Office, the Semiconductor Research Corporation (SRC), the National Science Foundation under grant EEC-0228930, and Purdue University. Work at Harvard was supported by Defense Advanced Research Projects Agency and Intel. We thank Raseong Kim, Kurtis Cantley, Sayeed Salahuddin, and Diego Kienle for helpful discussions. Computational support was provided by the Network for Computational Nanotechnology.

References

- (1) Xiang, J.; Lu, W.; Hu, Y.; Wu, Y.; Yan, H.; Lieber, C. M. *Nature* **2006**, *441*, 489.
- (2) Singh, N.; Agarwal, A.; Bera, L. K.; Liow, T. Y.; Yang, R.; Rustagi, S. C.; Tung, C. H.; Kumar, R.; Lo, G. Q.; Balasubramanian, N.; Kwong, D.-L. *IEEE Electron Device Lett.* **2006**, *27*, 383.
- (3) Goldberger, J.; Hochbaum, A. I.; Fan, R.; Yang, P. *Nano Lett.* **2006**, *6*, 973.
- (4) Duan, X.; Niu, C.; Sahi, V.; Chen, J.; Parce, J. W.; Empedocles, S.; Goldman, J. L. *Nature* **2003**, *425*, 274.
- (5) Li, Y.; Xiang, J.; Qian, F.; Gratecak, S.; Wu, Y.; Yan, H.; Blom, D. A.; Lieber, C. M. *Nano Lett.* **2006**, *6*, 1468.
- (6) Cui, Y.; Zhong, Z.; Wang, D.; Wang, W. U.; Lieber, C. M. *Nano Lett.* **2003**, *3*, 149.
- (7) Bjork, M.; Ohlsson, B.; Theflander, C.; Persson, A.; Depper, K.; Wallenberg, L.; Samuelson, L. *Appl. Phys. Lett.* **2002**, *81*, 4458.
- (8) Cui, Y.; Wei, Q.; Park, H.; Lieber, C. M. *Science* **2001**, *293*, 1289.
- (9) Hahn, J.; Lieber, C. M. *Nano Lett.* **2004**, *4*, 51.
- (10) Rahman, A.; Guo, J.; Datta, S.; Lundstrom, M. *IEEE Trans. Electron Devices* **2003**, *50*, 1853.
- (11) (a) Boykin, T.; Klimeck, G.; Oyafuso, F. *Phys. Rev. B* **2004**, *69*, 15201. (b) Klimeck, G.; Bowen, C.; Boykin, T. B.; Salazar-Lazaro, C.; Cwik, T. A.; Stoica, A. *Superlattices Microstruct.* **2000**, *27*, 77.
- (12) Lee, S.; Oyafuso, F.; Allmen, P.; Klimeck, G. *Phys. Rev. B* **2004**, *69*, 045316.
- (13) Wang, J.; Rahman, A.; Klimeck, G.; Lundstrom, M. *Tech. Dig.—Int. Electron Devices Meet.* **2005**, 530.
- (14) Sanders, G. D.; Chang, Y. C. *Appl. Phys. Lett.* **1992**, *60*, 2525.
- (15) Wang, J.; Rahman, A.; Ghosh, A.; Klimeck, G.; Lundstrom, M. *Appl. Phys. Lett.* **2005**, *86*, 093113.
- (16) Ilani, S.; Donev, L. A. K.; Kindermann, M.; McEuen, P. L. *Nat. Phys.* **2006**, *2*, 687.
- (17) Lundstrom, M.; Guo, J. *Nanoscale Transistors: Device Physics, Modeling and Simulation*; Springer: New York, 2005.
- (18) Guo, J.; Javey, A.; Dai, H.; Lundstrom, M. *Tech. Dig.—Int. Electron Devices Meet.* **2004**, 703.
- (19) Appenzeller, J.; Radosavljevi, M.; Knoch, J.; Avouris, Ph. *Phys. Rev. Lett.* **2004**, *92*, 048301.
- (20) Guo, J. Ph.D. Thesis, Purdue University, West Lafayette, IN, 2005.
- (21) Boykin, T. B.; Klimeck, G.; Bowen, R. C.; Oyafuso, F. *Phys. Rev. B* **2002**, *66*, 125207.
- (22) Klimeck, G.; Oyafuso, F.; Botkin, T. B.; Bowen, R. C.; Allmen, P. V. *Comput. Model. Eng. Sci.* **2002**, *3*, 601.
- (23) Gilbert, M. J.; Akis, R.; Ferry, D. K. *J. Appl. Phys.* **2005**, *98*, 094303.

NL062596F